Available online at www.sciencedirect.com
SCIENCE DIRECT®
International Journal of Heat and Mass Transfer 49 (2006) 1412–1419
International Journal of HEAT and MASS TRANSFER
www.elsevier.com/locate/ijhmt

The effect of axial diffusion in desiccant and enthalpy wheels

L.A. Sphaier, W.M. Worek *

Department of Mechanical and Industrial Engineering (M/C 251), University of Illinois at Chicago, Engineering Research Facility, 842 West Taylor Street, Chicago, IL 60607, United States

Received 1 April 2005; received in revised form 26 September 2005
Available online 13 December 2005

Abstract

A comparison between mathematical formulations for describing the transport phenomena occurring within desiccant and enthalpy wheels including axial heat and mass diffusion and a simplified version without these effects has been performed. Simulation results using a two-dimensional formulation were compared to determine under which conditions should these terms in fact be considered. The results include the variation of rotational speed, sorbent mass fraction, Biot numbers, and the aspect ratio of the porous desiccant substrate. The results show that the aspect ratio, together with the Biot numbers, are relevant parameters in determining whether axial diffusion should be included.

Keywords: Regenerator; Desiccant wheel; Enthalpy wheel; Dehumidification; Energy recovery

1. Introduction

The mathematical modeling of the transfer processes occurring within rotary dehumidifiers and enthalpy exchangers has been demonstrated to play an important role in enhancing the design and operation of these devices. The physical phenomena occurring in these devices involve coupled heat and mass transfer in the presence of physical adsorption. In order to better describe these processes in mathematical terms, different formulations have been adopted over the past years. Most formulations are composed of simple one-dimensional equations [1–6], in which the diffusional phenomena within the porous desiccant substrate are not locally considered. Some investigations adopt two-dimensional formulations, actually considering the thermal and mass diffusion in the desiccant substrate as local phenomena [7–12].

Some studies have included axial diffusion effects in their models [6,4,10–12], but most formulations apparently do not consider these terms. In some one-dimensional formulations [6,4] axial heat conduction is included due to the presence of a high conductivity supporting structure, which is considered lumped with the desiccant substrate. Other studies, using one-dimensional models, also consider [1,2] the supporting structure lumped with the sorbent material, but axial diffusion effects are not included. The model proposed in [11] includes axial heat and mass diffusion within the porous desiccant substrate; however equations for constant heat conductivity are employed. These terms may be necessary; nevertheless, their presence imply higher complexity in the equations and increased computational solution time. Although some of these studies consider axial diffusion and others do not, no comparison analyzing the effects of including or omitting these terms has been presented.

The purpose of this study is to investigate the effects of axial diffusion terms within the desiccant substrate and determine under which conditions could these terms be removed from the equations. The axial diffusion phenomena are studied isolated from parallel axial diffusion in a metallic supporting structure, by considering cases in which such a structure is omitted—such as in paper coated regenerators. In addition, this investigation also provides insight

* Corresponding author. Fax: +1 312 413 0447.
E-mail address: wworek@uic.edu (W.M. Worek).

0017-9310/$ - see front matter © 2005 Elsevier Ltd. All rights reserved.
doi:10.1016/j.ijheatmasstransfer.2005.09.035

Nomenclature

c, c_p	specific heats
$C^*_{r,f}$, C^*	sensible heat capacity ratios
Bi	Biot number
$\mathscr{D}^\star$	reference mass-diffusivity
f_s	mass fraction of sorbent in felt
Fi_T, Fo_T	Fick and Fourier numbers
i	specific enthalpy
i_{sor}	heat of sorption
i_{vap}	latent heat of vaporization
$i_{v,\Delta T}$	interface heat of sorbate transfer
k	thermal conductivity
K_f	felt aspect ratio (thickness/length)
Le	Lewis number
$N_{tu,o}$	overall number of transfer units
r, x, t	independent variables
T	temperature
$V^*_{r,f}$, V^*	volumetric capacity ratios
W	sorbate uptake
Y	sorbate content in gas mixture

Greek symbols

ϵ_f	felt porosity
Ω_{max}	dimensionless W^{max}_{fm}
Θ	dimensionless temperature
ρ	density or specific mass
τ_T	period of one full revolution
τ^*_{dw}	dimensionless dwell time
ϕ	molar fraction of sorbate in gas mixture
Φ	dimensionless sorbate concentration

Subscripts and superscripts

a	dry air
f	entire felt (matrix and pores)
fp	pores (inter-particle voids)
fm	matrix part of felt
p	process stream
fs	dry solid felt material
ls	saturated liquid sorbate
v	saturated sorbate vapor
*	dimensionless quantity
in, out	inlet and outlet
~	dry basis
I, II	processes streams I and II
h	related to sensible heat transfer
m	related to mass transfer
i	related to enthalpy transfer
p.s.	process stream/felt interface

on the amount of savings in computational time associated with using the simplified formulation.

2. Mathematical formulations

The heat and mass transfer processes occurring within rotary regenerators employing sorbent materials [12], in the absence of a supporting structure, can be described by the following governing equations:

$$\frac{1}{Fi_T}\left((1-\epsilon_f)f_s\Omega_{max}\frac{\partial\Phi_{fm}}{\partial t^*}+\epsilon_f\frac{\partial\Phi_{fp}}{\partial t^*}\right) = f_s\Omega_{max}\nabla_*\cdot(\delta_s\nabla_*\Phi_{fm})+\nabla_*\cdot(\delta_g\nabla_*\Phi_{fp}), \quad (1)$$

$$\frac{\chi_f}{Fo_T}\frac{\partial\Theta_f}{\partial t^*}=\nabla_*\cdot(\kappa_f\nabla_*\Theta_f)+\frac{i^*_{sor}f_s\Omega_{max}}{Le_f}\times\left(\frac{1}{Fi_T}(1-\epsilon_f)\frac{\partial\Phi_{fm}}{\partial t^*}-\nabla_*\cdot(\delta_s\nabla_*\Phi_{fm})\right), \quad (2)$$

$$\tau^*_{dw}\frac{D\Phi_p}{Dt^*}=(1+V^*)N^m_{tu,o}(\Phi_{fp}|_{p.s.}-\Phi_p), \quad (3)$$

$$\chi_p\tau^*_{dw}\frac{D\Theta_p}{Dt^*}=(1+C^*)N^h_{tu,o}(\Theta_f|_{p.s.}-\Theta_p), \quad (4)$$

and the following boundary conditions:

$$-f_s\Omega_{max}\delta_s\frac{\partial\Phi_{fm}}{\partial r^*}-\delta_g\frac{\partial\Phi_{fp}}{\partial r^*}=Bi_m(\Phi_p-\Phi_{fp}), \quad (5)$$

$$-\kappa_f\frac{\partial\Theta_f}{\partial r^*}=Bi_h(\Theta_p-\Theta_f)+\frac{Bi_m}{Le_f}(\Phi_p-\Phi_{fp})i^*_{v,\Delta T}-\frac{f_s\Omega_{max}}{Le_f}\delta_s\frac{\partial\Phi_{fm}}{\partial r^*}i^*_{sor}, \quad (6)$$

at the interface $r^*=0$, and

$$\left(\frac{\partial\Phi_{fp}}{\partial r^*}\right)_{r^*=1}=\left(\frac{\partial\Theta_f}{\partial r^*}\right)_{r^*=1}=0,\quad \left(\frac{\partial\Phi_{fp}}{\partial x^*}\right)_{x^*=0}=\left(\frac{\partial\Theta_f}{\partial x^*}\right)_{x^*=0}=0,\quad \left(\frac{\partial\Phi_{fp}}{\partial x^*}\right)_{x^*=1}=\left(\frac{\partial\Theta_f}{\partial x^*}\right)_{x^*=1}=0. \quad (7–9)$$

at the remaining boundaries. The dimensionless Del operator (∇_*), present in the previous equations, is used in its two-dimensional form with Cartesian coordinates:

$$\nabla_*=\left(K_f\frac{\partial}{\partial x^*},\frac{\partial}{\partial r^*},0\right), \quad (10)$$

Also, the material derivative is given by

$$\frac{D}{Dt^*}=\frac{\partial}{\partial t^*}+\frac{1}{\tau^*_{dw}}\frac{\partial}{\partial x^*}, \quad (11)$$

and the local equilibrium relation is written as

$$\Phi_{fm}=\Phi_{fm}(\Theta_f,\Phi_{fp}). \quad (12)$$

Furthermore, the normalized periodic inlet conditions are given by

$$\left.\begin{aligned}&\Phi_p(0,t^*)=\Phi^I_{in}(t^*),\quad \Theta_p(0,t^*)=\Theta^I_{in}(t^*),\quad \text{for } 0\leqslant t^*\leqslant\tfrac{\tau_1}{\tau_T}\\ &\Phi_p(0,t^*)=\Phi^{II}_{in}(t^*),\quad \Theta_p(0,t^*)=\Theta^{II}_{in}(t^*),\quad \text{for } \tfrac{\tau_1}{\tau_T}\leqslant t^*\leqslant 1\end{aligned}\right\}\quad \text{for } N=1,2,\ldots \quad (13–16)$$

where N corresponds to the number of revolutions, and—in each of these—the dimensionless process time t^* varies from 0 to 1. In addition, the change of variable

$$x^*_{\text{next}} = 1 - x^*_{\text{current}}, \tag{17}$$

is applied at the end of each process for a counterflow configuration.

The previous formulation can be significantly simplified if the effects of axial diffusion, comprising heat conduction, gas-phase diffusion and surface diffusion terms in the x-direction, are considered negligible and removed from the governing equations. This simplification is usually justified by the fact that the aspect ratio K_f is sufficiently small and that there is no flux at the boundaries $x^* = 0$ and $x^* = 1$, resulting in the following modification to the ∇_* operator

$$\nabla_* = \left(0, \frac{\partial}{\partial r^*}, 0\right), \tag{18}$$

which reduces Eqs. (1) and (2) to:

$$\frac{1}{Fi_T}\left((1-\epsilon_f) f_s \Omega_{\max} \frac{\partial \Phi_{fm}}{\partial t^*} + \epsilon_f \frac{\partial \Phi_{fp}}{\partial t^*}\right) = f_s \Omega_{\max} \frac{\partial}{\partial r^*}\left(\delta_s \frac{\partial \Phi_{fm}}{\partial r^*}\right) + \frac{\partial}{\partial r^*}\left(\delta_g \frac{\partial \Phi_{fp}}{\partial r^*}\right), \tag{19}$$

Table 1
Input data used in simulations

$c_{p_a} = 1007$ J/kg °C	$k_a = 0.0263$ W/m °C
$c_{p_v} = 1872$ J/kg °C	$k_v = 0.0196$ W/m °C
$c_{ls} = 4180$ J/kg °C	$k_l = 0.613$ W/m °C
$c_{fs} = 920$ J/kg °C	$k_{fs} = 0.24$ W/m °C
$\mathscr{D}^{\star}_p = 2.94 \times 10^{-5}$ m^2/s	$\mathscr{D}^{\star}_f = 3.43 \times 10^{-6}$ m^2/s
$\rho_a = 1.1614$ kg/m^3	$\rho_{fs} = 800$ kg/m^3
$\epsilon_f = 0.40$	$W^{\max}_{fm} = 0.40$ kg/kg
$C^*_{r,f} = 20/\tau_T$	$\tau^*_{dw} = 0.08/\tau_T$
$C^* = 1.0$	$i_{sor} = 1.2 \times i_{vap}$
$T^{I}_{in} = 15$ °C	$T^{II}_{in} = 30$ °C
$\phi^{I}_{in} = 40\%$	$\phi^{II}_{in} = 40\%$
$T_{ref} = 15$ °C	$\Delta T_{ref} = 15$ °C
$Y_{ref} = 4.2625$ g/kg	$\Delta Y_{ref} = 6.4654$ g/kg

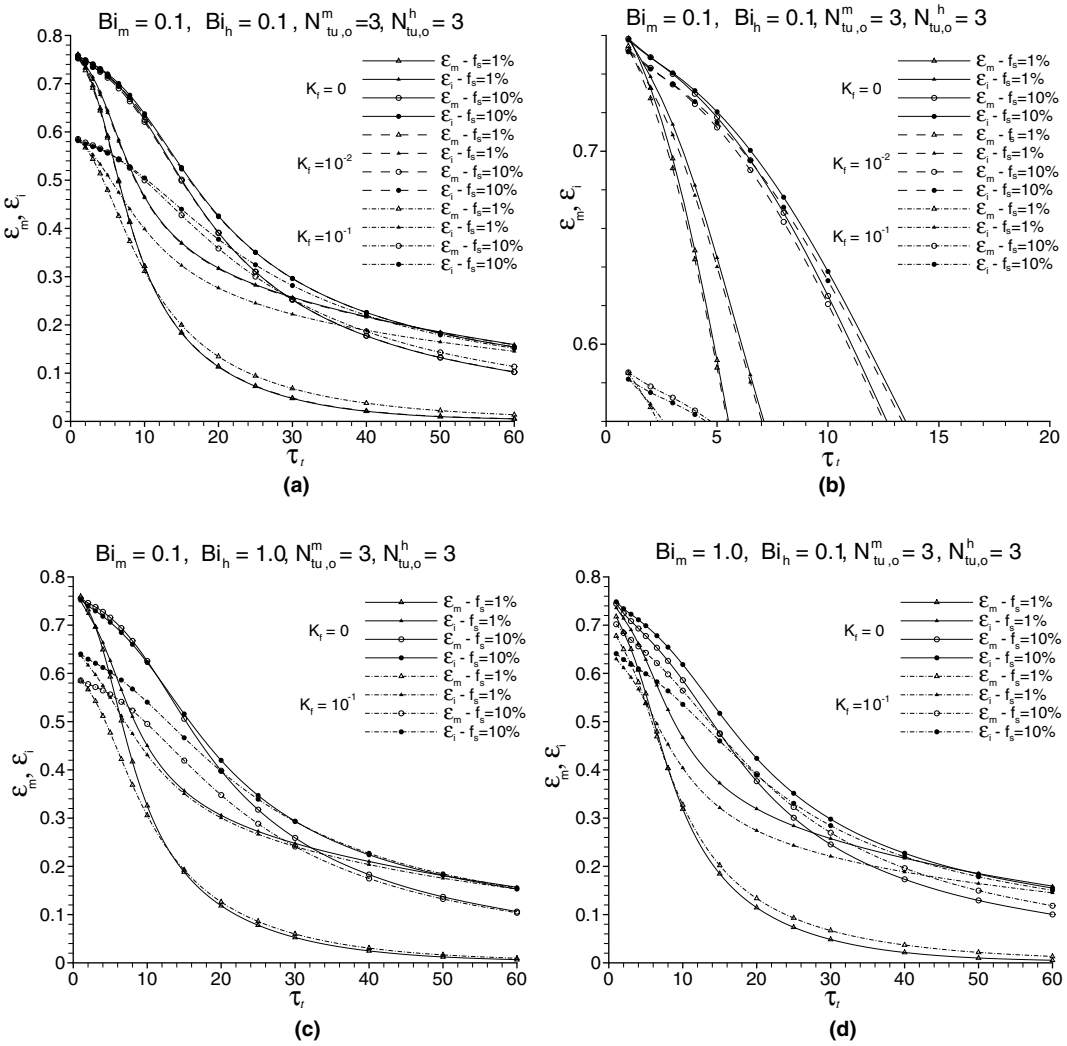

Fig. 1. Influence of K_f on the performance results for different cases, with $N^h_{tu,o} = 3$ and $N^m_{tu,o} = 3$—smaller Biot numbers.

$$\frac{\chi_f}{Fo_T}\frac{\partial \Theta_f}{\partial t^*} = \frac{\partial}{\partial r^*}\left(\kappa_f \frac{\partial \Theta_f}{\partial r^*}\right) + \frac{i^*_{sor} f_s \Omega_{max}}{Le_f}\left(\frac{1}{Fi_T}(1-\epsilon_f)\frac{\partial \Phi_{fm}}{\partial t^*} - \frac{\partial}{\partial r^*}\left(\delta_s \frac{\partial \Phi_{fm}}{\partial r^*}\right)\right). \quad (20)$$

However, the required magnitude of K_f to validate this simplification should be determined. The dimensionless parameters in the presented equations are related through

$$Fi_T = \frac{(1+V^*)^2}{V^*}\frac{N^m_{tu,o}}{Bi_m V^*_{r,f}}, \quad (21)$$

$$Fo_T = \frac{(1+C^*)^2}{C^*}\frac{N^h_{tu,o}}{Bi_h C^*_{r,f}}, \quad (22)$$

$$Le_f = \frac{Fo_T}{Fi_T}, \quad (23)$$

$$C^* = V^*. \quad (24)$$

The expressions for calculating the coefficients i^*_{sor}, $i^*_{v,\Delta T}$, χ_p, χ_f, δ_s, δ_g, and κ_f, as well as a detailed explanation of the dimensionless parameters, are provided in [12].

3. Results and discussion

The equations herein presented were computationally solved using a combination of two numerical methods: finite volumes and the numerical method of lines. All grids were sufficiently refined to ensure acceptable levels of precision, and the magnitude of the relative error in the mass and energy balances between both inlet and outlet streams was less than 10^{-3}.

To assess the overall performance of the regenerator, three types of effectiveness—temperature, mass and enthalpy—are employed. These are respectively defined as

$$\varepsilon_t = \frac{\overline{\Theta}^{out}_{p,I} - \Theta^{in}_{p,I}}{\Theta^{in}_{p,II} - \Theta^{in}_{p,I}}, \quad (25)$$

$$\varepsilon_m = \frac{\overline{\Phi}^{out}_{p,I} - \Phi^{in}_{p,I}}{\Phi^{in}_{p,II} - \Phi^{in}_{p,I}}, \quad (26)$$

$$\varepsilon_i = \frac{\overline{\tilde{i}}^{out}_{p,I} - \tilde{i}^{in}_{p,I}}{\tilde{i}^{in}_{p,II} - \tilde{i}^{in}_{p,I}}, \quad (27)$$

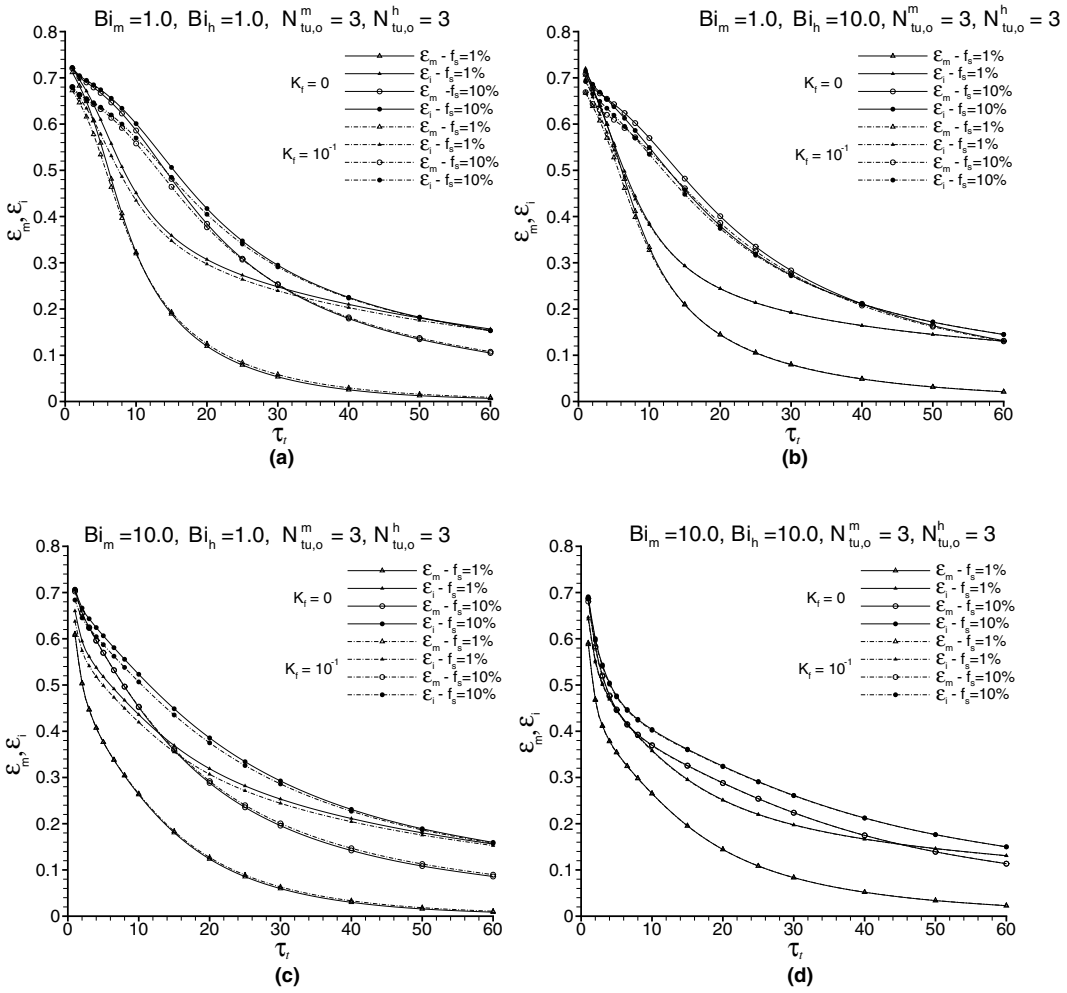

Fig. 2. Influence of K_f on the performance results for different cases, with $N^h_{tu,o} = 3$ and $N^m_{tu,o} = 3$—larger Biot numbers.

where,

$$\overline{\Theta}^{\text{out}}_{\text{p,I}} = \frac{1}{\tau_{\text{I}}}\int_0^{\tau_{\text{I}}} \Theta^{\text{out}}_{\text{p,I}}\,\mathrm{d}t^*, \tag{28}$$

$$\overline{\Phi}^{\text{out}}_{\text{p,I}} = \frac{1}{\tau_{\text{I}}}\int_0^{\tau_{\text{I}}} \Phi^{\text{out}}_{\text{p,I}}\,\mathrm{d}t^*, \tag{29}$$

$$\bar{\bar{i}}^{\text{out}}_{\text{p,I}} = \frac{1}{\tau_{\text{I}}}\int_0^{\tau_{\text{I}}} \bar{i}^{\text{out}}_{\text{p,I}}\,\mathrm{d}t^*, \tag{30}$$

The calculation of the above enthalpies will depend on reference values of physical properties, and detailed information on calculating these enthalpies can be found in [12].

In order to investigate the effects of omitting the axial diffusion terms, the results obtained with $K_{\text{f}} = 0$, i.e. Eqs. (19) and (20), were compared with the ones calculated with Eqs. (1) and (2) for different values of K_{f}. Different values for the sorbent concentration in the porous felt f_{s} were used, and the dimensional process time τ_T, which directly affects the dimensionless parameters $C^*_{\text{r,f}}$ and τ^*_{dw} was varied from 1 to 60 s. Table 1 shows this dependence and also provides the reference values for physical properties and the dimensionless parameters that were held fixed. The reference physical properties of the desiccant substrate employed are typical to a silica-gel desiccant. In addition, the overall numbers of transfer units ($N^{\text{h}}_{\text{tu,o}}$ and $N^{\text{m}}_{\text{tu,o}}$) were varied from 1 to 3, and different Biot numbers Bi_{m} and Bi_{h} were employed: 0.1, 1.0, and 10.0.

Figs. 1 and 2 compare the solutions with $K_{\text{f}} = 0$ (no axial diffusion) with $K_{\text{f}} = 10^{-1}$ and $K_{\text{f}} = 10^{-2}$, for a varying τ_T and different values of f_{s}. Different configurations of Biot numbers are presented and the numbers of transfer units are held constant at $N^{\text{h}}_{\text{tu,o}} = N^{\text{m}}_{\text{tu,o}} = 3$. The curves for $K_{\text{f}} = 10^{-2}$, in all cases but the one with $Bi_{\text{m}} = Bi_{\text{h}} = 1.0$, perfectly coincide with the curves for $K_{\text{f}} = 0$, and they are only displayed for this case. Fig. 1b shows the same curves presented in Fig. 1a within a smaller scale for better visualizing the $K_{\text{f}} = 10^{-2}$ curves. The results clearly indicate that the difference between the different K_{f} curves increases with decreasing Biot numbers. In fact, for $Bi_{\text{m}} = Bi_{\text{h}} = 10$, the K_{f} curves nearly overlap each other. In addition, while the greater discrepancy occurs for $K_{\text{f}} = 10^{-1}$, the remaining cases are practically equivalent to the case without axial

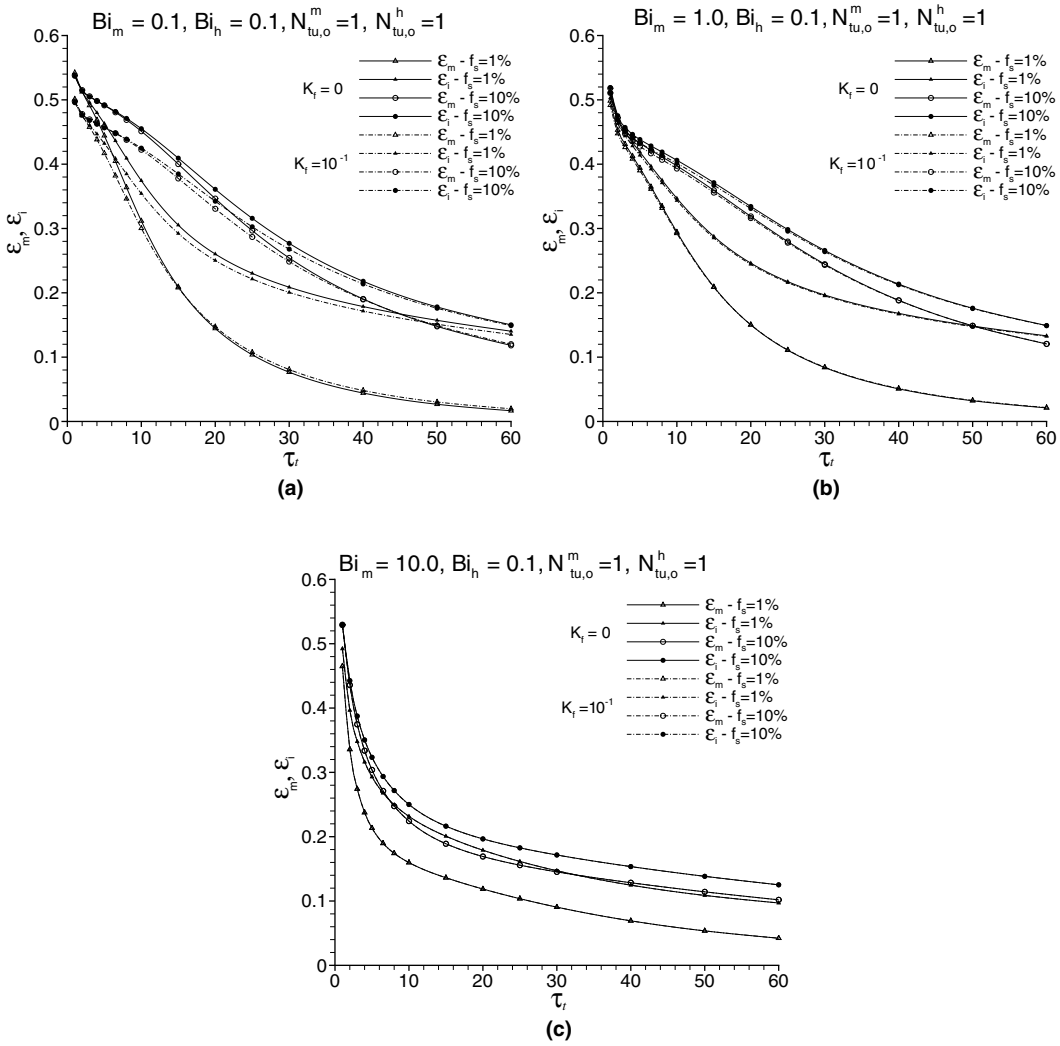

Fig. 3. Influence of K_{f} on the performance results for different cases, with $N^{\text{h}}_{\text{tu,o}} = 1$ and $N^{\text{m}}_{\text{tu,o}} = 1$.

diffusion. Fig. 3 provides an analogous comparison for $N^{h}_{tu,o} = N^{m}_{tu,o} = 1$, illustrating a similar trend. Besides varying the number of transfer units, the effect of changing the inlet conditions was also investigated. However, the same trend was observed.

In order to illustrate the advantage of removing the axial diffusion terms from the equations, the computational time of *single-blow* solutions with different values of K_f (with $K_f = 0$ implying no axial diffusion) are compared. These solutions correspond to solving the proposed problem from $t^* = 0$ to $t^* = 1$ with the following inlet and initial conditions:

$$\Phi_p(0,t^*) = 1, \quad \Theta_p(0,t^*) = 1, \qquad \text{for } 0 \leqslant t^* \leqslant 1, \quad (31,32)$$

$$\Phi_p(x^*,0) = 0, \quad \Theta_p(x^*,0) = 0, \qquad \text{for } 0 \leqslant x^* \leqslant 1. \quad (33,34)$$

The results of these simulations are shown in Fig. 4, indicating that the removal of the axial diffusion terms from the equations generally produces a reduction in the computational time in excess of 20%. In addition, the relative error in the integral mass and energy balances between the porous sorbent and the process stream were calculated for these cases, always yielding values of magnitude less than 10^{-4}.

Although the presented results compare the effectiveness for cases with and without axial diffusion, the question of whether the potentials in the felt (i.e. sorbate concentration and temperature) also behave in a similar way needs to be analyzed. Table 2 displays numerical data for the case with $Bi_m = Bi_h = 1$, $N^{h}_{tu,o} = N_{tu,m} = 3$ and $f_s = 0.1\%$, including the sorbate concentration and temperature in the felt (averaged value, shown at $t^* = 1$), together with the outlet potentials at $t^* = 1$, and the CPU time. As can be seen, the data indicate that for $K_f = 10^{-2}$, the solution practically yields the same numbers as the formulation without axial solution ($K_f = 0$). Also, for the case with $K_f = 10^{-1}$, the solution is still generally very close to the case with no axial diffusion, with some noticeable discrepancy; however, as discussed previously, this case presents an exaggeration of a real configuration. Hence, the effect observed in the effectiveness results, is again observed for the potentials within the felt.

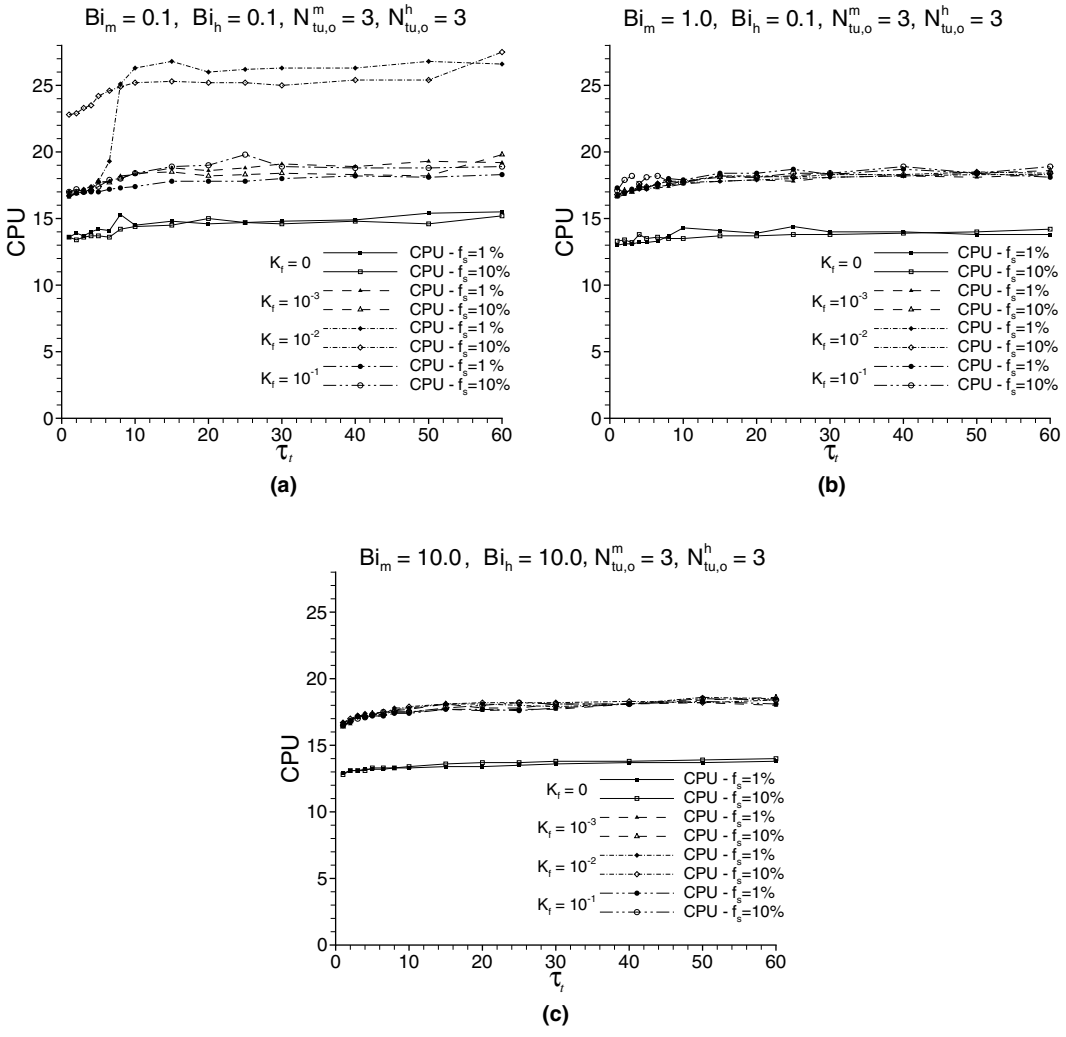

Fig. 4. Computational time (CPU in seconds) of single-blow simulations.

Table 2
Tabulated data from solution of case with $f_s = 0.1\%$, $Bi_m = Bi_h = 1$ and $N^m_{tu,o} = N^h_{tu,o} = 3$

K_f	τ_T	$\Theta^1_{p,out}$	$\Phi^1_{p,out}$	$\overline{\Theta}^1_f$	$\overline{\Phi}^1_{fp}$	ε_m	ε_i	CPU
0	1	0.6801	0.1399	0.4724	0.0686	0.5907	0.6580	2.37E+3
10^{-2}	1	0.6795	0.1400	0.4724	0.0689	0.5903	0.6575	2.58E+3
10^{-1}	1	0.6361	0.1463	0.4735	0.0874	0.5613	0.6212	1.97E+3
0	5	0.5916	−0.0100	0.4024	−0.0074	0.1206	0.3898	4.00E+2
10^{-2}	5	0.5911	−0.0100	0.4024	−0.0074	0.1206	0.3895	5.26E+2
10^{-1}	5	0.5553	−0.0093	0.4079	−0.0072	0.1211	0.3708	5.28E+2
0	10	0.5016	−0.0090	0.3239	−0.0063	0.0518	0.3447	2.51E+2
10^{-2}	10	0.5012	−0.0090	0.3240	−0.0063	0.0518	0.3445	3.49E+2
10^{-1}	10	0.4712	−0.0084	0.3340	−0.0063	0.0526	0.3266	3.36E+2
0	15	0.4122	−0.0078	0.2518	−0.0052	0.0294	0.3221	1.81E+2
10^{-2}	15	0.4119	−0.0078	0.2520	−0.0052	0.0295	0.3219	2.52E+2
10^{-1}	15	0.3878	−0.0074	0.2658	−0.0053	0.0303	0.3050	2.63E+2
0	30	0.1781	−0.0040	0.0931	−0.0022	0.0092	0.2632	1.24E+2
10^{-2}	30	0.1780	−0.0040	0.0933	−0.0022	0.0092	0.2630	1.71E+2
10^{-1}	30	0.1766	−0.0040	0.1131	−0.0026	0.0099	0.2505	2.02E+2
0	60	0.0115	−0.0003	0.0048	−0.0001	0.0031	0.1600	8.50E+1
10^{-2}	60	0.0116	−0.0003	0.0049	−0.0001	0.0031	0.1600	1.20E+2
10^{-1}	60	0.0207	−0.0005	0.0127	−0.0003	0.0032	0.1575	1.25E+2

4. Summary and conclusions

This work investigated the effects of axial heat and mass diffusion occurring within the porous desiccant substrate contained in rotary regenerators, such as desiccant and enthalpy wheels. The effect of this phenomena, isolated from diffusion in a adjacent highly conductive metallic layer, was studied by employing a formulation in which such metallic structure is absent. The equations were computationally solved and the error involved in the numerical solution process was assessed by evaluating integral mass and energy balances.

In order to reduce the mathematical complexity and computational solution time, the original formulation proposed in [12] was simplified by assuming by assuming negligible axial heat and mass diffusion. The validity of the given equations was investigated, showing that for higher Biot numbers and slower rotational speeds (i.e. longer τ_T) this additional approximation can be considered with minor errors. The discrepancy between the complete and simplified equations was also shown to increase with increasing K_f—especially for $K_f \geqslant 0.1$. However, values within this range are an exaggeration of real configurations, which indicates that, in general, axial diffusion within the sorbent felt could be considered negligible. The only exception would be in the cases of extremely low Biot numbers combined with higher values of K_f, which encompasses rotors having thicker desiccant substrates with elevated thermal conductivity. The presented results also illustrate that about 20% of solution time can be spared if axial diffusion is not considered.

Overall, the results provided in this investigation can be applied for achieving a more effective mathematical formulation, in which accurate computational simulations can be performed in the minimum amount of time possible.

Acknowledgement

The authors would like to acknowledge the financial support provided by, CNPq (Brazil) and the University of Illinois at Chicago.

References

[1] D. Charoensupaya, W.M. Worek, Parametric study of an open-cycle adiabatic, solid, desiccant cooling system, Energy 13 (9) (1988) 739–747.
[2] W. Zheng, W.M. Worek, Numerical simulation of combined heat and mass transfer processes in rotary dehumidifier, Numer. Heat Transfer, Part A 23 (1993) 211–232.
[3] H. Klein, S.A. Klein, J.W. Mitchell, Analysis of regenerative enthalpy exchangers, Int. J. Heat Mass Transfer 33 (4) (1990) 735–744.
[4] C.J. Simonson, R.W. Besant, Heat and moisture transfer in desiccant coated rotary energy exchangers: Part I. Numerical model, HVAC & R Research 3 (4) (1997) 325–350.
[5] G. Stiesch, S.A. Klein, J.W. Mitchell, Performance of rotary heat and mass exchangers, HVAC & R Research 1 (4) (1995) 308–323.
[6] C.J. Simonson, R.W. Besant, Energy wheel effectiveness—part I: development of dimensionless groups, Int. J. Heat Mass Transfer 42 (1999) 2161–2170.
[7] D. Charoensupaya, W.M. Worek, Effect of adsorbent heat and mass transfer resistances on performance of an open-cycle adiabatic desiccant cooling system, Heat Recovery Syst. CHP 8 (6) (1988) 537–548.
[8] P. Majumdar, W.M. Worek, Combined heat and mass transfer in a porous adsorbent, Energy 14 (3) (1989) 161–175.
[9] P. Majumdar, Heat and mass transfer in composite pore structures for dehumidification, Solar Energy 62 (1) (1998) 1–10.
[10] J.L. Niu, L.Z. Zhang, Effects of wall thickness on the heat and moisture transfers in desiccant wheels for air dehumidification and enthalpy recovery, Int. Commun. Heat Mass Transfer 29 (2) (2002) 255–268.

[11] J.L. Niu, L.Z. Zhang, Performance comparisons of desiccant of desiccant wheels for air dehumidification and enthalpy recovery, Appl. Thermal Eng. 22 (2002) 1347–1367.

[12] L.A. Sphaier, W.M. Worek, Analysis of heat and mass transfer in porous sorbents used in rotary regenerators, Int. J. Heat Mass Transfer 47 (2004) 3415–3430.